Modulation of Actin Affinity and Actomyosin Adenosine Triphosphatase by Charge Changes in the Myosin Motor Domain †

ARTICLE *in* BIOCHEMISTRY · MAY 1998

Impact Factor: 3.02 · DOI: 10.1021/bi972851y · Source: PubMed

3 AUTHORS, INCLUDING:

Michael A Geeves
University of Kent
231 PUBLICATIONS **7,655** CITATIONS

SEE PROFILE

Dietmar J Manstein
Hannover Medical School
148 PUBLICATIONS **4,582** CITATIONS

SEE PROFILE

Modulation of Actin Affinity and Actomyosin Adenosine Triphosphatase by Charge Changes in the Myosin Motor Domain†

Marcus Furch,‡ Michael A. Geeves,§ and Dietmar J. Manstein*,‡

Max-Planck-Institut für Medizinische Forschung, Jahnstrasse 29, D-69120 Heidelberg, Germany, and Max-Planck-Institut für Molekulare Physiologie, Postfach 102664, D-44026 Dortmund, Germany

Received November 20, 1997; Revised Manuscript Received January 28, 1998

ABSTRACT: The effects of mutations in an actin-binding surface loop of myosin (loop 2) are described. Part of loop 2, the segment between myosin residues 618 and 622, was replaced with sequences enlarged by the introduction of positively charged GKK or neutral GNN motifs. Constructs with loops carrying up to 20 additional amino acids and charge variations from −1 to +12 were produced. Steady-state and transient kinetics were used to characterize the enzymatic behavior of the mutant motor domains. Binding of nucleotide was not affected by any of the alterations in loop 2. In regard to their interaction with actin, constructs with moderate charge changes (−1 to +2) displayed wild-type-like behavior. Introduction of more than one GKK motif led to stronger coupling between the actin- and nucleotide-binding sites of myosin and an up to 1000-fold increased affinity for actin in the absence of ATP and at zero ionic strength. In comparison to the wild-type construct M765, constructs with 4−12 extra charges displayed an increased dependence on ionic strength in their interaction with actin, a 2−3-fold increase in k_{cat}, a more than 10-fold reduction in K_{app} for actin, and a 34−70-fold increase in catalytic efficiency.

The members of the myosin superfamily form a large and diverse group of molecular motors that power a wide range of contractile events in eukaryotic cells. All myosins contain a motor domain that generates force in an unidirectional manner relative to filamentous actin through the hydrolysis of ATP.[1] A neck region that provides binding sites for one or more calmodulin/EF-hand superfamily light chains connects this generic motor domain with unique and functionally specialized tail domains. The amino acid sequence of all myosin motor domains show a high degree of conservation and can be aligned in primary sequence with the *Dictyostelium discoideum* myosin II or chicken skeletal muscle myosin sequences, for which structural data at atomic resolution are available (*1*, *2*). The structures of the myosin motor domains from *D. discoideum* and chicken skeletal muscle are remarkably similar. Both structures share a common backbone, and major changes in length and sequence composition are restricted to surface regions. Similarly, sequence alignments with other myosin motor domains show that deletions or insertions occur at positions that correspond to surface segments in the structures.

The two surface segments that have received most attention lie in proteolytically sensitive regions that have been used to cleave the myosin head into 25, 50, and 20 kDa polypeptides. The first surface loop, termed loop 1, is located near the ATP binding pocket at the 25−50 kDa junction. Loop 2 is at the 50−20 kDa junction and forms part of the actin binding site. Since myosins from diverse species and cell types show great variability in enzymatic and motile activity, the hypothesis was put forward that these poorly conserved loop regions play an important role in determining the enzymatic properties of myosins (*3*). Although there is some disagreement about the specific effects of changes in the loops on motility and ATPase activity, their importance in modulating the enzymatic activity of myosin was clearly demonstrated in a number of studies (*4*−*9*).

The interaction between actin and myosin is thought to proceed through three steps (*10*). After the initial formation of a weakly specific collision complex that is dominated by long-range electrostatic interactions, an attached (A-state) low-affinity complex is formed. This complex isomerizes, which leads to the formation of a high-affinity complex (R-state). The A-state is in equilibrium with the R-state and the equilibrium position is determined by the nucleotide bound to the myosin motor. Binding of ATP to the R-state results in dissociation of actin. Hydrolysis of ATP followed by product dissociation leads to repopulation of the R-state. Structural and biochemical studies indicate that loop 2 and the negatively charged N-terminal part of actin are mainly responsible for the long-range electrostatic interactions leading to the formation of the collision complex (*11*−*14*) and several site-directed mutagenesis studies on actin

† Supported by the Max-Planck-Society and the DFG.

* To whom correspondence should be addressed: Tel. (+49-6221) 486 212; Fax (+49-6221) 486 437; e-mail manstein@mpimf-heidelberg.mpg.de.

‡ Max-Planck-Institut für Medizinische Forschung.

§ Max-Planck-Institut für Molekulare Physiologie.

[1] Abbreviations: acto•M, complex of actin and myosin head fragment; ATP, adenosine 5′-triphosphate; DTT, 1,4-dithiothreitol; EDTA, ethylenediaminetetraacetic acid; EGTA, ethylene glycol bis(2-aminoethyl ether)-*N*,*N*,*N*′,*N*′-tetraacetic acid, kb, kilobase(s); HMM, heavy meromyosin; LDH, lactate dehydrogenase: MHF, myosin head fragment; MHC, myosin heavy chain; *mhc*A, gene encoding myosin heavy chain; MOPS, 3-(*N*-morpholino)propanesulfonic acid; NADH, nicotinamide adenine dinucleotide; ORF, open reading frame; PCR, polymerase chain reaction; PEP, phosphoenolpyruvate; pyr-actin, pyrene-labeled actin; PK, pyruvate kinase; S1, subfragment 1 of myosin.

S0006-2960(97)02851-1 CCC: $15.00
Published on Web 04/14/1998

Table 1: Introduction of GNN and GKK Motifs into the 50K/20K Junction[a]

native sequence: AAA CTT TTC AAT GAT CCA AAC ATT [GCC AGT CGT GCA AAG] AAA GGT GCA AAC

^{610}K L F N D P N I [A S R A K] K G A N^{626}

mutant construct	introduced amino acid sequence	Δ length/charge	MW (Da)
M765(4/−1)	G N N G A S R A Q	4/1−	89 536
M765(5/−1)	G N N G A S N R A Q	5/1−	89 664
M765(8/0)	G N N G A R G N N G R A Q	8/0	89 947
M765(11/0)	G N N G A R G N N G N N G R A Q	11/0	90 233
M765(4/+1)	G K K G A S R A Q	4/1+	89 797
M765(5/+2)	G K K G A S K R A Q	5/2+	89 692
M765(8/+4)	G K K G A R G K K G R A Q	8/4+	90 004
M765(11/+6)	G K K G A R G K K G K K G R A Q	11/6+	90 317
M765(20/+12)	G K K G A R G K K G K K [G K K]$_3$ G R A Q	20/12+	91 258

[a] Amino acid residues 618−622 of the native sequence, shown in brackets at the top of the table, were replaced in mutant constructs with neutral or positively charged sequences listed below for each of the constructs. The naming of the mutant motor domain constructs reflects changes in the length and charge of loop 2.

confirmed the importance of the N-terminal negative charges of actin for the interaction with myosin (*15*−*17*).

The importance of loop 2 in tuning the enzymatic activity of myosin was investigated in two studies by chimeric replacement of the native loop with that from other myosins. Replacement of the native loop of smooth muscle heavy meromyosin with that from either skeletal or β-cardiac myosin caused the chimaeric HMMs to become unregulated like the myosin from which the loop was derived, without affecting the affinity of HMM for actin in the presence of MgATP or k_{cat}, the maximum turnover rate in the presence of actin (*7*). Chimeras composed of the *D. discoideum* myosin II backbone and loop 2 regions from myosins from other species showed actin-activated ATPase activities that correlate well with the activity of the myosins from which the loop sequences were derived (*6*). For example, loop substitution with rabbit skeletal muscle sequences made the enzyme 5−6-fold more active as measured by the k_{cat} of its actin-activated ATPase activity (*3*). While these studies confirmed the critical role of loop 2 in "tuning" the enzymatic activity of myosins, it remained unclear what exact features of the loop account for an increase or decrease in enzymatic activity.

In the present work, we used site-directed mutagenesis of *D. discoideum* myosin head fragment M765, a soluble myosin head fragment truncated after residue 765, and kinetic measurements to study the effect of changes in the loop 2 region. M765 shows kinetic behavior similar to that of an S1-like *D. discoideum* myosin head fragment (*18*, *19*). The interaction of M765 with nucleotide and actin follows the same basic mechanism and the kinetics can be analyzed in the same way described for S1 from rabbit fast muscle myosin and other muscle myosins (*20*). Nine mutant constructs were generated to systematically dissect the effect of size and charge changes in the loop sequence and to correlate them with the enzymatic behavior of the myosin motor domain. The segment between *D. discoideum* myosin residues 618 and 622 was replaced with sequences enlarged by the introduction either of several neutral GNN or positively charged GKK motifs (Table 1, Figure 1). Mutant constructs with loops carrying up to 20 additional amino acids and charge variations from −1 to +12, in comparison to native *Dictyostelium* myosin, were produced and characterized.

MATERIALS AND METHODS

Plasmid Construction. All subcloning was done using standard procedures (*21*). Plasmids for the production of recombinant myosin motor domains were derived from the extrachromosomal vector pDXA-3H (*22*) and were amplified in *Escherichia coli* strain XL1 Blue (Stratagene, Heidelberg, Germany). Plasmid pDH20 was used for the expression of M765 under the control of the *D. discoideum actin 15* promoter. M765 includes the first 765 residues of the *D. discoideum mhcA* gene and carries a C-terminal His tag. Plasmids encoding M765 with specific loop 2 replacements were created by PCR-directed mutagenesis (*23*). Three oligonucleotides were used for the PCR reactions: a mutagenic primer and two nonmutagenic oligonucleotides that prime from either site to the mutation, outside of unique *Bst*XI and *Xho*I sites in plasmid pM765. The PCR mutagenesis was carried out in two steps. First, a 5′ fragment was synthesized using the common 5′-primer mhc1600 (AGAAGAACGCCAAATACGAAGAACCAC) and one of the mutagenic primers. Next, the resulting 230 bp fragment was gelpurified and employed as 5′-megaprimer in a second PCR with M769NC (CATGGCTCGAGTGATTTCAGAGATACGTTGTTCACGAGC) as 3′-primer. The resulting ∼650 bp fragment was digested with *Bst*XI/*Xho*I and subcloned into the *Bst*XI and *Xho*I sites of pM765. The following mutagenic primers were used (all sequences are shown 5′ to 3′, and mutated sequences are underlined): M765(4/-1), AGTGATAAAGTTTGCACCTTTCTGAGCTCGACTGGCACCATTATTACCAATGTTTGGATCATTGAAAAGTTTGGT: M765(4/+1), AGTGATAAAGTTTGCACCTTTCTGAGCTCGACTGGCACCTTTCTTACCAATGTTTGGATCATTGAAAAGTTTGGT; M765(5/−1), AGTGATAAAGTTTGCACCTTTCTGAGCTCGATTGCTAGCACCATTATTACCAATCTTTGGATCATTGAAAAGTTTGGT; M765(5/+2), AGTGATAAAGTTTGCACCTTTCTGAGCTCGTTTGCTAGCACCTTTCTTACCAATGTTTGGATCATTGAAAAGTTTGGT. In addition to the changes in the coding sequence of the resulting constructs, the mutagenesis resulted in the creation of a unique *Sac*I

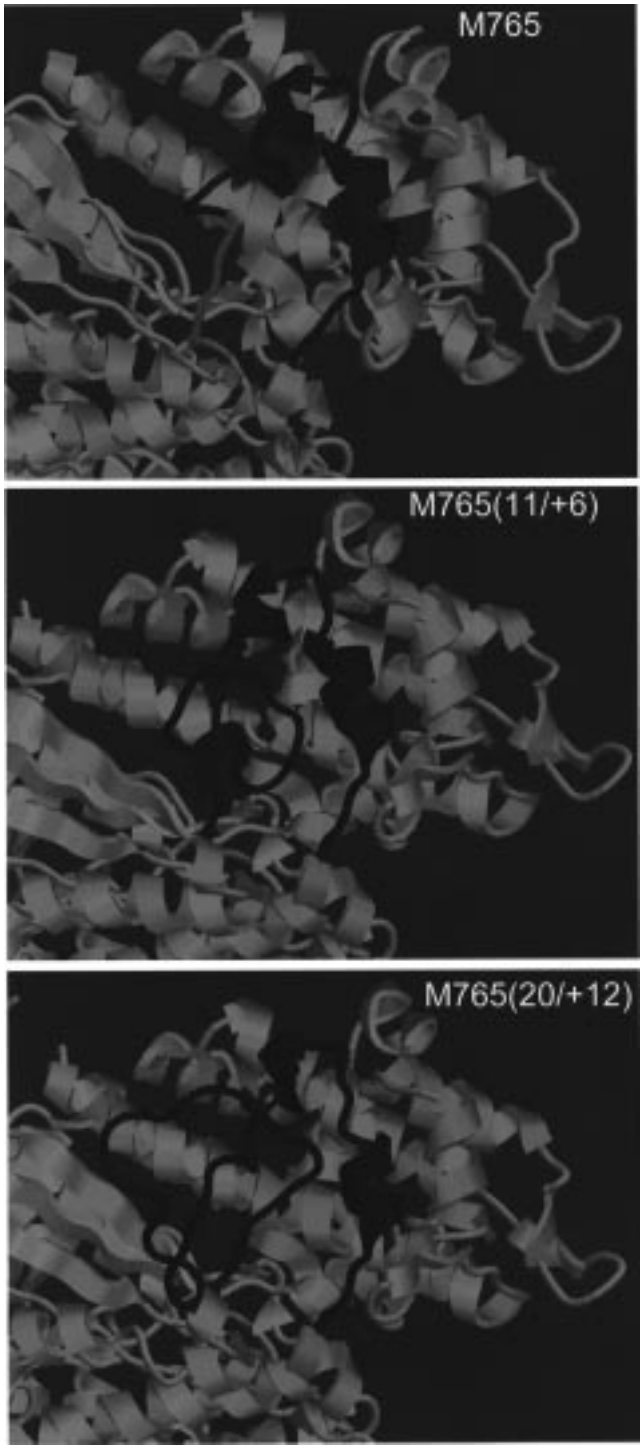

FIGURE 1: Close-up view of the actin binding region of the *D. discoideum* motor domain (*2*) and the modeled actin binding regions of M765(11/+6) and M765(20/+12). The region between wild-type residues Pro-591 and Lys-623 is shown in blue, except for the representation of M765, where the region that was replaced in the mutant constructs (residues Ala-618−Lys-622) is shown in orange. SegMod (*41*) was used for homology modeling of the mutant loop structures, and the figure was prepared using the molecular visualization program RasMol (*42*)

site in all plasmids and a unique *Nhe*I site in pM765(5/−1) and pM765(5/+2). Vectors for the production of M765(8/0) and M765(11/0) were generated by insertion of annealed oligonucleotide pairs into the *Sac*I/*Nhe*I sites of pM765(5/−1). Vectors for the production of M765(8/+4), M765(11/+6), and M765(20/+12) were created by inserting annealed oligonucleotide pairs into the S*ac*I/*Nhe*I sites of pM765(5/+2). The oligonucleotides were annealed and ligated without phosphorylation to ensure insertion of a single copy. The following oligonucleotide pairs were used: CTAGGGGTAATAATGGTCGAGCT (ns-2n−c) and CGACCATTATTACCC (ns-2n−n) for the creation of pM765(8/0); CTAGGGGTAATAATGGTAATAATGGTCGAGCT (ns-4n-c) and CGACCATTATTACCATTATTACC (ns-4n-c) for pM765(11/0). The sequences of the oligonucleotide pairs used for the construction of the pM765(5/+2)-derived plasmids were CTAGGGGTAAGAAAGGTCGAGCT (ns-7/3+c) and CGACCTTTCTTACCC (ns-7/3+n) for pM765(8/+4); CTAGGGGTAAGAAAGGTAAAAAAGGTCGAGCT (ns-10/+5c) and CGACCTTTTTTACCTTTCTTACCC (ns-10/+5n) for pM765(11/+6); and CTAGGGGTAAGAAAGGTAAAAAAGGTAAGAAAGGTAAGAAAGGTAAGAAAGGTCGAGCT (k5+c) and CGACCTTTCTTACCTTTCTTACCTTTCTTACCTTTTTTACCTTTCTTACCC (k5+n) for pM765(20/+12). Ligation of the oligonucleotide pairs into the *Nhe*I/*Sac*I digested vector destroyed the *Nhe*I site, thus facilitating screening of transformants for the presence of the inserts using diagnostic *Nhe*I/*Xho*I digests. Additionally, all DNA constructs were verified by sequencing.

Strains and Growth Conditions. D. discoideum transformants were grown at 21 °C in HL-5C containing (per liter): 5 g of protease peptone (Merck), 5 g, of Bacto yeast extract (Difco), 2.5 g of Bacto tryptone (Difco), 2.5 g of casein peptone (Merck), 10 g of D-glucose, 0.35 g of Na_2HPO_4, and 1.2 g of KH_2PO_4 (pH 6.5). Cells were either grown on 9 cm plastic Petri dishes or in 100 mL conical flasks on a gyratory shaker at 190 rpm. Plasmids were transformed into Orf^+ cells (*22*) by electroporation (*24*). Transformants were selected and continuously grown in the presence of 20 μg/mL of the aminoglycoside G418 (Gibco BRL). Transformants were screened for the production of the recombinant myosin motor domains as described previously (*25*).

Protein Purification. Cells producing the mutant myosin motor domains were grown in 5 L flasks containing 2.5 L of HL-5C. The flasks were incubated on gyratory shakers at 200 rpm and 21 °C. Cells were harvested at a density of about 7.5×10^6 mL^{-1} by centrifugation for 7 min at 2700 rpm in a Beckman J-6 centrifuge and washed once in phosphate-buffered saline. The His-tagged motor domains were purified as described by Manstein and Hunt (*25*). The purified protein could be stored at −80 °C for several months without apparent loss of enzymatic activity.

Rabbit actin was purified by the method of Lehrer and Kewar (*26*) with minor modifications. Briefly, no ATP was added at the final step to polymerize actin and residual amounts of nucleotide were removed by sequential centrifugation of actin and dialysis steps. Actin was labeled with pyrene (pyr-actin) as previously described (*27*). The concentration of the recombinant *D. discoideum* myosin motor domains was determined by Bradford assay.

Stopped-Flow Experiments and Fluorescence Titrations. Stopped-flow experiments for transient kinetics were performed at 20 °C with a Hi-tech Scientific SF61 or SF-61MX stopped-flow spectrophotometer. The observation cells of both systems have a 10 mm excitation path and fluorescence emission via 10×1.5 mm^2 windows. Pyrene fluorescence

was excited at 365 nm and detected after passage through a KV 389-nm cutoff filter. Data were stored and analyzed using software provided by Hi-tech. Transients shown are the average of 3−5 consecutive shots of the stopped-flow machine. All concentrations refer to the concentration of the reactants after mixing in the stopped-flow observation cell. Fluorescence titrations were carried out on a SLM 8000 spectrofluorometer at 20 °C using excitation/emission bandwidths of 4 nm. Pyrene fluorescence was excited at 365 nm with emission at 405 nm. Typical working volumes of 700 μL were used. The experimental buffer used for transient kinetic experiments was 20 mM MOPS, 5 mM $MgCl_2$, and 100 mM KCl, pH 7.0, unless stated otherwise.

Steady-State ATPase. We modified the PK/LDH-linked ATPase assay described by Trentham and co-workers (*28*) for the stopped-flow instrument. NADH oxidation was followed using fluorescence (excitation at 340 nm; emission through a KV 389-nm cutoff filter). The assay was performed at 25 °C in a buffer containing 25 mM imidazole, 25 mM KCl, and 4 mM $MgCl_2$. Myosin constructs were added to one syringe of the stopped-flow instrument, while the other syringe contained 0.5 mM DTT, 0.5 mM ATP, 0.2 mM NADH, 0.5 mM phosphoenolpyruvate (PEP), 0.02 mg/mL lactate dehydrogenase (LDH), and 0.05 mg/mL pyruvate kinase (PK). Actin activation of myosin ATPase activity was measured either by adding actin to one or both syringes. Identical results were obtained under both conditions. The highest concentration of actin used per syringe was 160 μM and the highest concentration following mixing was 100 μM actin. Following mixing, the change in NADH fluorescence was recorded for periods of up to 1000 s.

The signal change attributable to photobleaching was less than 2% of the total change in fluorescence intensity during this period. No significant differences were observed from one actin preparation to another and the assay was not affected by free ADP from the actin preparation. A burst of NADH oxidation at the start of the reaction, due to the presence of free ADP, was never observed.

All measurements were carried out at several myosin concentrations, as shown for M765(8/+4) in Figure 2A. Steady state rates of fluorescence change were plotted as a linear function of myosin construct concentration and converted to ATPase rates using a standard curve. The results obtained using the linked enzyme assay were generally in good agreement with those obtained using the colorimetric assay described by White (*29*). The linked assay has, however, the advantage that it requires smaller amounts of the myosin constructs and the results show less variability, particularly in the range from 50 to 100 μM actin.

RESULTS

Purification of Mutant Myosin Motor Domains. High synthesis levels were obtained with M765 and all mutant constructs described in this study. The histidine-tagged recombinant proteins were purified to homogeneity by binding to actin and release with ATP followed by Ni^{2+}-chelate affinity chromatography. Up to 3 mg of homogeneous protein/g of cells was obtained after purification. The mutant constructs did not behave significantly different from wild-type construct M765 in this purification.

Steady-State ATPase Assays. All mutant constructs were able to hydrolyze ATP at least as fast as M765. In the absence of actin we determined a basal ATPase activity of 0.08 s^{-1} for M765. Most of the mutant constructs displayed a similar or slightly elevated basal ATPase activity. The values measured for individual constructs varied between 0.06 and 0.25 s^{-1} (Table 2).

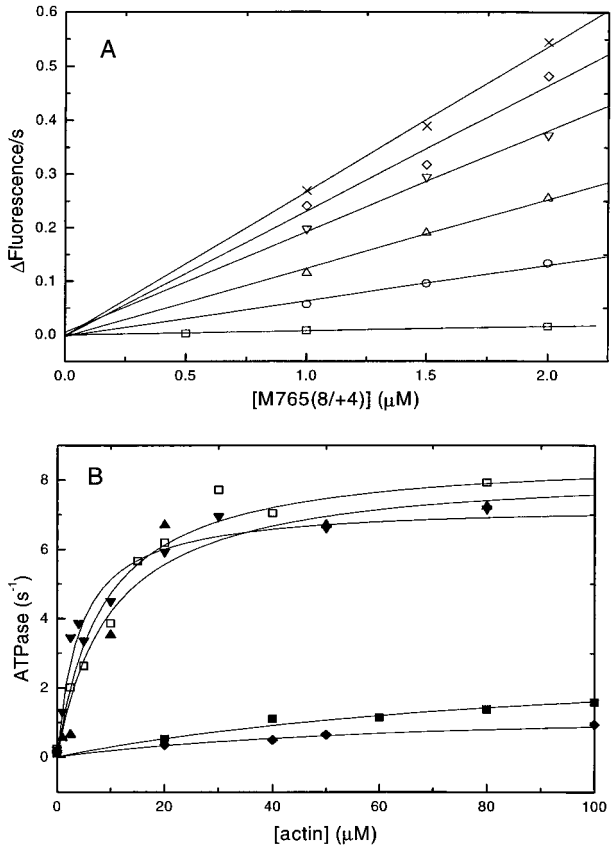

FIGURE 2: Dependence of steady-state ATPase on myosin and actin concentration. A linked assay system was used in the stopped-flow instrument, and NADH turnover was followed by excitation at 340 nm. Fluorescence emission was observed through a KV 389 filter. Conditions: 25 mM imidazole, 25 mM KCl, 4 mM $MgCl_2$, 0.5 mM DTT, 0.5 mM ATP, 0.2 mM NADH, 0.5 mM PEP, 0.02 mg/mL LDH, and 0.05 mg/mL PK, pH 7.4. (A) Mg^{2+}-ATPase assays were performed at actin concentrations of 0 μM (□, basal), 2.5 μM (○), 10 μM (△), 15 μM (▽), 40 μM (◇), and 80 μM (×) and initiated by addition of M765(8/+4). The steady-state part of the resulting curves was fitted to a straight line. The slopes were linearly dependent upon myosin concentration in the range from 0.5 to 2 μM. Steady-state rates of fluorescence change were converted to ATPase rates using a standard curve. (B) Actin-activated ATPase activities of M765 (■), M765(5/−1) (◆), M765 (8/+4) (□), M765 (11/+6) (▲), and M765 (20/+12) (▼) measured at varying concentrations of rabbit skeletal muscle actin. Values up to 100 μM actin were determined. The observed rates were plotted against actin concentration and fitted to a hyperbola, giving the Michaelis parameters summarized in Table 2.

Actin-activated ATPase measurements were initially performed in the presence of 20 μM actin and at an ionic strength of $I = 0.06$ M. A value of 0.53 s^{-1} was determined for M765 under these conditions, which corresponds to a 5.6-fold activation. Myosin constructs with minimal changes of charge in the loop 2 region (−1 to +2) showed only marginal differences in the actin-activated ATPase in the range from 0.34 to 0.77 s^{-1}. In terms of activation, however, activation by 20 μM actin was more variable for these constructs (1.6−6.5-fold across the series). Lower activation was always associated with elevated basal ATPase activity.

Table 2: Steady-State Kinetic Parameters

myosin construct	Mg^{2+}-ATPase[a] basal (s^{-1})	Mg^{2+}-ATPase[a] actin-activated (s^{-1})	Mg^{2+}-ATPase[a] activation	Michaelis parameter[b] k_{cat} (s^{-1})	Michaelis parameter[b] K_{app} (μM)	catalytic efficiency, k_{cat}/K_{app} (M^{-1} s^{-1})
M765(wild type)	0.08 ± 0.02	0.53 ± 0.02	5.6	2.6 ± 1	102 ± 20	0.25×10^5
M765(4/−1)	0.13 ± 0.03	0.34 ± 0.03	1.6	nd	>100	0.09×10^5
M765(5/−1)	0.17 ± 0.04	0.44 ± 0.03	1.6	2.3 ± 1.5	172 ± 70	0.13×10^5
M765(8/0)	0.06 ± 0.02	0.38 ± 0.03	5.3	nd	>100	0.10×10^5
M765(11/0)	0.25 ± 0.04	0.77 ± 0.05	2.1	nd	>100	0.25×10^5
M765(4/+1)	0.09 ± 0.02	0.68 ± 0.04	6.5	nd	>100	0.29×10^5
M765(5/+2)	0.17 ± 0.04	0.44 ± 0.03	1.6	nd	>100	0.12×10^5
M765(8/+4)	0.21 ± 0.04	6.20 ± 0.18	28.5	8.7 ± 0.3	8.5 ± 1.0	10.2×10^5
M765(11/+6)	0.17 ± 0.04	6.69 ± 0.22	38.4	8.3 ± 0.6	9.9 ± 0.8	8.4×10^5
M765(20/+12)	0.18 ± 0.04	5.17 ± 0.35	27.7	7.2 ± 0.5	4.1 ± 0.9	17.6×10^5

[a] Actin-activated Mg^{2+}-ATPase activity was measured in the presence of 20 μM rabbit skeletal muscle F-actin. ATPase activation = (actin-activated ATPase − basal ATPase)/basal ATPase. [b] Values for k_{cat} and K_{app} were calculated from fitting the data to the Michaelis−Menten equation. Values for k_{cat}/K_{app} were calculated from the initial slope. All measurements were performed at 25 °C.

Much greater levels of actin activation were seen for the three constructs with four or more extra lysine residues in the loop. Actin (20 μM) elevated the ATPase for M765(8/+4) 29-fold to a value of 6.20 s^{-1}, for M765(11/+6) 38-fold to 6.69 s^{-1}, and for M765(20/+12) 28-fold to 5.17 s^{-1}.

To determine whether this effect resulted from an increase in k_{cat} (the maximum turnover rate in the presence of actin) or from a decrease of K_{app} (the apparent K_M for actin), ATPase assays were performed over a wider range of actin concentrations. The ATPase activity of M765 and constructs with an increase in charge of less than 4 displayed a linear dependence up to the highest actin concentration used (100 μM). K_{app} was therefore estimated for all of these constructs as greater than 100 μM, yielding values for k_{cat} of $\geq$2.3 s^{-1}. In contrast, for constructs with $\geq$4 charges, the actin-dependence of the ATPase activity could be described by a hyperbola and yielded values of K_{app} < 10 μM and k_{cat} of approximately 8 s^{-1} (Figure 2).

At concentrations of actin much lower than K_{app}, the dependence of the apparent ATPase rate on actin concentration can be fitted to a straight line and the catalytic efficiency (k_{cat}/K_{app}) of the reaction can be determined from the slope of this line. The k_{cat}/K_{app} of M765 was determined to be 0.25×10^5 M^{-1} s^{-1}, which is similar to the value of 0.28×10^5 M^{-1} s^{-1} measured for an S1-like *D. discoideum* myosin construct by Giese and Spudich (*30*). Mutant constructs with loop 2 inserts carrying 4−12 extra positive charges showed a clear increase in catalytic efficiency. Compared to the wild-type construct M765, the increase was 40-fold (10.2×10^5 M^{-1} s^{-1}) for M765(8/+4), 33-fold (8.4×10^5 M^{-1} s^{-1}) for M765(11/+6), and 70-fold (17.6×10^5 M^{-1} s^{-1}) for M765(20/+12). All other constructs showed only minor changes in catalytic efficiency (Table 2).

Actin Binding to the Mutant Constructs. The rate of actin binding was monitored by observing the exponential decrease of the pyrene fluorescence that follows mixing of the mutant myosin constructs with an excess of pyrene-labeled actin (pyr-actin). The fluorescence of the pyrene reporter group is quenched by ~70% upon binding of *D. discoideum* myosin head fragments (*18*). Figure 3 shows the transient records obtained after mixing 0.25 μM M765, M765(4/+1), or M765(8/+4) with an excess of pyr-actin. The solid lines superimposed on each transient represent the best fit to a biexponential. The slower rate was not affected by the reaction temperature or changes in the concentration of actin and had a constant value identical to the rate of the signal change that was caused by photobleaching of the pyrene label under our experimental conditions. The values for the faster rate (k_{obs}) were plotted against the actin concentration and were linear over the concentration range from 0.5 to 2.5 μM actin. In every case the intercepts were indistinguishable from zero, consistent with a much slower rate of actin dissociation than the k_{obs} values recorded here. The second-order association rate constants (k_{on}) obtained from the slopes are listed in Table 3 for all constructs. The second-order rate constants for M765(4/−1), M765(5/−1), M765(8/0), and M765(11/0) differ by less than 10% from the value determined for wild-type construct M765 (1.34×10^6 M^{-1} s^{-1}). The insertion of one or two extra positive charges had a greater effect, leading to an increase of k_{on} by 60% and 25% for M765(4/+1) and M765(5/+2), respectively. However, the largest changes in k_{on} were observed for mutant constructs carrying inserts with four or more additional positive charges in loop 2. For M765(8/+4), k_{on} increased by a factor of 5, for M765(11/+6) 7-fold, and for M765(20/+12) 8-fold.

Dissociation of the Actomyosin Complex in the Absence of ATP. The rate constant for actin dissociation from the various myosin motor domain constructs (k_{off}) was determined by chasing pyr-actin with an excess of unlabeled actin. Figure 4 shows the time course for displacement of pyr-actin from 0.5 μM pyr-acto·M by addition of 20 μM unlabeled actin taken on a stopped-flow spectrophotometer. The pyr-actin is completely displaced from M765(5/−1) after 400 s, while for M765(8/+4) and M765(11/+6) the reaction is still far from completion. To obtain precise k_{obs} values for the slow-dissociating constructs, the reactions were performed in a spectrofluorometer on an extended time scale of up to 6000 s (see insert in Figure 4). The observed process of the increase in pyrene fluorescence could be fitted to a single exponential where k_{obs} corresponds directly to k_{off} (Table 3). The dissociation rate constant was essentially invariant for all constructs except M765(8/+4), M765(11/+6), and M765(20/+12), for which k_{off} was reduced 5-, 10-, and 17-fold in comparison to M765.

Affinity of the Myosin Constructs for Actin. The dissociation equilibrium constant (K_d) for actin binding to different mutant constructs was calculated from the ratios of k_{off} and k_{on} (*27*, *31*). Additionally, K_ds greater than 1 nM were measured directly by the method described previously (*32*). The results obtained by both methods were generally in good agreement.

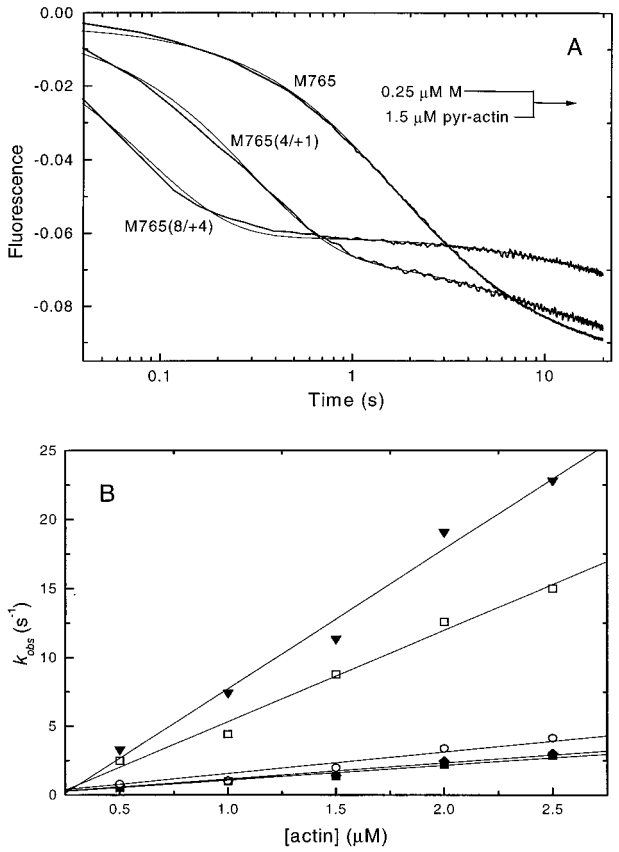

FIGURE 3: Rate of pyr-actin binding to myosin motor domain constructs. (A) Stopped-flow record of the change in pyrene fluorescence following the mixing of 1.5 μM pyr-actin with 0.25 μM myosin motor domain construct (all concentrations refer to the concentration of the reactants after mixing in the stopped-flow observation cell). Pyrene fluorescence was excited at 365 nm and emission was observed through a KV 389 filter. The time course of the fluorescence decrease after mixing myosin constructs and pyr-actin fits a biexponential. (B) Dependence of the rate of the observed processes on pyr-actin concentration. The data were fitted to a straight line, the slope of which gives a second-order binding constant (k_{on}). The intercepts are all near zero since the rate of dissociation is slower than the rate of association determined by these plots. Values of 1.34 M^{-1} s^{-1} [M765(wt)], 1.40 M^{-1} s^{-1} [M765(11/0)], 2.16 M^{-1} s^{-1} [M765(4/+1)], 7.11 M^{-1} s^{-1} [M765(8/+4)], and 10.89 M^{-1} s^{-1} [M765(20/+2)] were determined. The symbols correspond to the following *D. discoideum* myosin constructs: M765(wt) (■), M765 (5/−1) (◆), M765 (4/+1) (○), M765 (8/+4) (□), and M765 (20/+12) (▼). Conditions: 20 mM Mops, 5 mM $MgCl_2$, and 100 mM KCl, pH 7.0, 20 °C.

Our results show that the actin affinity of six out of nine mutant constructs is similar to that of the wild-type construct M765. Only constructs carrying inserts with four or more additional positive charges in loop 2 show a clear increase in affinity for actin. For M765(8/+4), M765(11/+6), and M765(20/+12), we determined dissociation equilibrium constants for actin binding that are 30-, 60-, and 120-fold smaller than the value determined for M765.

ATP-Induced Dissociation of Actomyosin Motor Domain Complexes. The binding of ATP to pyr-actin-bound myosin constructs was monitored by observing the exponential increase in pyrene fluorescence as the complex dissociates following addition of excess ATP (see Figure 5A). The observed rate constants were linearly dependent upon ATP concentration in the range from 5 to 25 μM as shown in Figure 5B. ATP binding was analyzed in terms of the model shown in Scheme 1. In this scheme A and M represent actin and myosin motor domain constructs, respectively.

Scheme 1

$$A{\cdot}M + ATP \overset{K_1}{\rightleftharpoons} A{\cdot}M{\cdot}ATP \xrightarrow{k_{+2}} A + M{\cdot}ATP \rightarrow$$

The first step is a rapid equilibrium between A·M and ATP defined by the equilibrium constant K_1. This is followed by an isomerization of the ternary complex that limits the maximum rate of actin dissociation from the complex. Thus the observed rate constant for the ATP-induced dissociation of actin from the complex is defined by

$$k_{obs} = K_1 k_{+2}[ATP]/(1 + K_1[ATP])$$

If $K_1[ATP] \ll 1$, then $k_{obs} = K_1 k_{+2}[ATP]$ and the apparent second-order binding constant $K_1 k_{+2}$ is defined by the slope. These were similar for all constructs ($2.4 \pm 0.5 \times 10^5$ M^{-1} s^{-1}). This experiment shows that the various loop 2 insertions do not affect nucleotide binding or communication between the actin and nucleotide site.

Influence of Ionic Strength on the Formation of the Actomyosin Complex. It is well-known that the affinity of actin for myosin or S1 is dependent on the ionic strength (*33*−*35*) with both the affinity of actin for S1 and the rate of S1 binding increasing at lower ionic strength. We measured k_{on} and k_{off} at different salt concentrations for M765, M765(8/+4), M765(11/+6), and M765(20/+12). At the lowest ionic strength used ($I = 0.03$ M), k_{on} for M765 was 3.0×10^6 M^{-1} $s^{-1}$and increasing the ionic strength up to 0.53 decreased k_{on} to 4.6×10^5 M^{-1} s^{-1}. Table 3 shows the values at standard ionic strength of $I = 0.13$ M. In contrast, k_{off} for M765 was relatively insensitive to changes in ionic strength and showed a value of 0.008 s^{-1} at $I =$ 0.53 M.

The ionic strength dependence of k_{on} and k_{off} is shown in Debye−Hückel plots in Figure 6. The Debye−Hückel relationship applies to small ions at low salt conditions and is therefore not strictly applicable to the investigation of ionic interaction of two proteins. However, the plot of log k against the square root of the ionic strength exhibits a linear dependence for rabbit S1 (*35*, *36*) and as shown in Figure 6 for the *D. discoideum* myosin motor domain constructs used here. The plot of log k_{on} against the square root of the ionic strength gave a slope of −1.27 $M^{-0.5}$ for M765 and slopes of −3.1 $M^{-0.5}$ for M765(8/+4), M765(11/+6), and M765(20/+12). Plots of log k_{off} against $\sqrt{I}$ produced almost parallel lines with the following slopes: 0.43 $M^{-0.5}$ for M765, 0.67 $M^{-0.5}$ for M765(8/+4), 0.78 $M^{-0.5}$ for M765(11/+6), and 0.70 $M^{-0.5}$ for M765(20/+12).

The intercepts with the log k axis define values for k_{on} and k_{off} at zero ionic strength. For M765(8/+4), M765(11/+6), M765(20/+12), the predicted value for k_{on} at zero ionic strength is 19-, 34-, and 45-fold faster than for the wild-type construct M765 [$(4.2 \pm 3) \times 10^6$ $M^{-1}s^{-1}$], while the predicted value for k_{off} at zero ionic strength is 6-, 10-, and 16-fold slower than the corresponding value for M765 [$(4.4 \pm 1) \times 10^{-3}$ s^{-1}]. The rate and equilibrium constants at zero ionic strength are summarized in Table 4 for the individual constructs.

Table 3: Transient Kinetic Analysis[a]

	actin binding to myosin constructs			ATP binding to acto·M
myosin construct	k_{on} (M^{-1} s^{-1})	k_{off} (s^{-1})	$K_d = k_{off}/k_{on}$ (nM)	$k_{+2}K_1$ (M^{-1} s^{-1})
M765(wild type)	1.34×10^6	6.8×10^{-3}	4.8	2.5×10^5
M765(4/−1)	1.22×10^6	8.0×10^{-3}	6.4	2.8×10^5
M765(5/−1)	1.22×10^6	8.3×10^{-3}	5.8	2.8×10^5
M765(8/0)	1.37×10^6	5.0×10^{-3}	3.7	2.8×10^5
M765(11/0)	1.40×10^6	5.0×10^{-3}	3.6	nd
M765(4/+1)	2.16×10^6	6.6×10^{-3}	2.9	nd
M765(5/+2)	1.67×10^6	5.4×10^{-3}	3.3	2.7×10^5
M765(8/+4)	7.11×10^6	1.3×10^{-3}	0.16	2.5×10^5
M765(11/+6)	8.93×10^6	0.7×10^{-3}	0.08	1.9×10^5
M765(20/+12)	10.89×10^6	0.4×10^{-3}	0.04	2.1×10^5

[a] Experimental conditions for all measurements: 20 mM MOPS, 5 mM $MgCl_2$, and 100 mM KCl, pH 7.0, 20 °C.

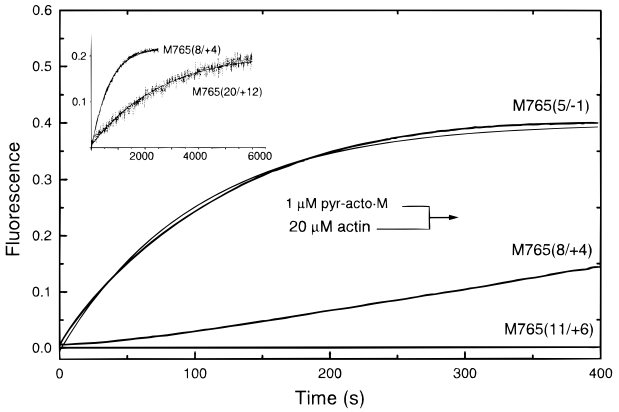

FIGURE 4: Determination of the rate of actin displacement from acto·M. The dissociation rate constants (k_{off}) was determined from the rate of fluorescence enhancement when excess unlabeled actin was added to a sample of 0.5 μM pyr-actin equilibrated with an equimolar amount of mutant myosin construct. The stopped flow records of M765(5/−1), M765(8/+4), and M765(11/+6) are shown. Due to the slow progress of the reaction the k_{off} values for M765(8/+4), M765(11/+6), and M765(20/+12) had to be determined with the aid of an SLM 8000 spectrofluorometer. The insert shows the traces for M765(8/+4) and M765(20/+12), as recorded with the spectrofluorometer, on an extended time scale. The solid lines are the best fit to a single-exponential defining values for k_{off} shown in Table 3. Conditions: 20 mM Mops, 5 mM $MgCl_2$, and 100 mM KCl, pH 7.0, 20 °C.

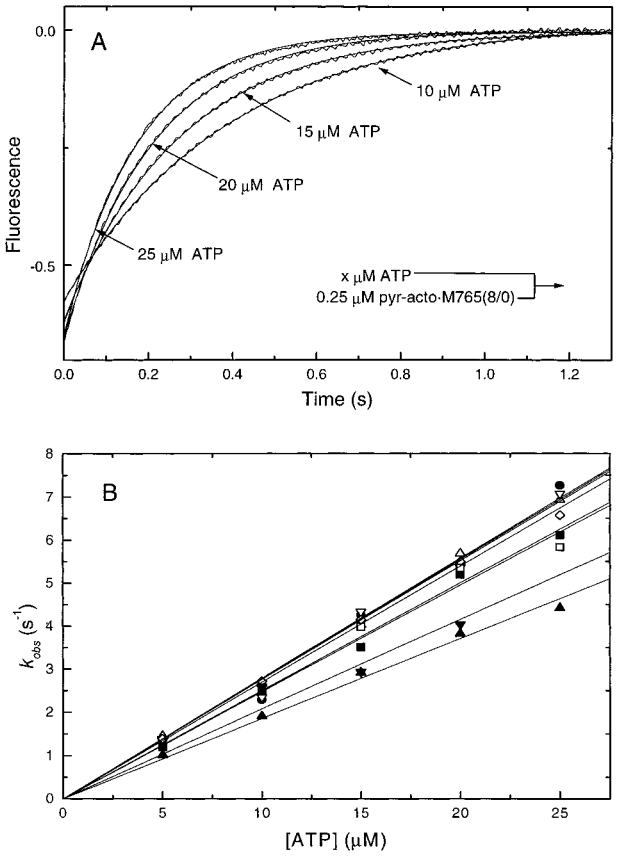

FIGURE 5: ATP-induced dissociation of pyr-acto·M complexes. (A) Fluorescence changes observed when 0.5 μM pyr-acto·M765(8/0) was mixed with 10, 15, 20, or 25 μM ATP. The best fits to single-exponential functions are shown superimposed and the observed rate constants are plotted in panel B. The observed rate constants were linear over the range 5−25 μM ATP. The second-order rate constant of ATP binding to the acto·M complex is defined by the gradient. The fitted parameters are listed in Table 3. The symbols correspond to the following *D. discoideum* myosin fragment mutants: M765 (■), M765 (4/−1) (△), M765 (5/−1) (◆), M765 (8/0) (▽), M765 (5/+2) (◇), M765 (8/+4) (□), M765 (11/+6) (▲), and M765 (20/+12) (▼). Conditions: 20 mM Mops, 5 mM $MgCl_2$, and 100 mM KCl, pH 7.0, 20 °C.

DISCUSSION

The data presented here on the loop 2 mutants shows that the myosin head is remarkably insensitive to changes in the structure of this loop, provided the total charge in the loop is changed by not more than 2 units of charge. Inserting an extra length of 8 or 11 amino acids, with no additional charge, produced no measurable effect on the myosin or actomyosin ATPase, the rate of ATP binding to the actin-bound myosin head, or the rate or equilibrium constants of association between actin and myosin motor. A similar result was observed for loops with four or five additional amino acids with −1, +1, or +2 charges. The only exception to this was that the value of k_{on} for actin binding was 60% higher for the M765(4/+1) construct compared to the parent M765.

In contrast, addition of four or more basic amino acids to the loop produced drastic changes in the interaction between actin and myosin motor domain. Constructs M765(8/+4), M765(11/+6), and M765(20/+12) showed the same basal ATPase rates and the same rate of ATP-induced dissociation of the complex with actin, consistent with no major change in the properties of the nucleotide binding site. Only the interaction with actin was affected, which is consistent with loop 2 being a primary interaction site between myosin and actin. Both the K_d for actin binding and the K_{app} were decreased 10−120-fold for M765(8/+4), M765(11/+6), and M765(20/+12). In the case of the affinity for a nucleotide-free head this was due to both an increase in the association rate constant (k_{on}) by a factor of 5−8 and a decrease in the

Table 4: Rate and Equilibrium Constants for the Interaction of Actin with Myosin Constructs at Zero Ionic Strength

	M765	M765(8/+4)	M765(11/+6)	M765(20/+12)
k_{on}^0 (M^{-1} s^{-1} $\times$ 10^6)	4.2 ± 3	80 ± 30	145 ± 25	190 ± 40
k_{off}^0 (s^{-1} $\times$ 10^{-3})	4.4 ± 1	0.76 ± 0.3	0.43 ± 0.1	0.27 ± 0.6
$K_d^0 = k_{off}^0/k_{on}^0$ (pM)	1000	10	3	1

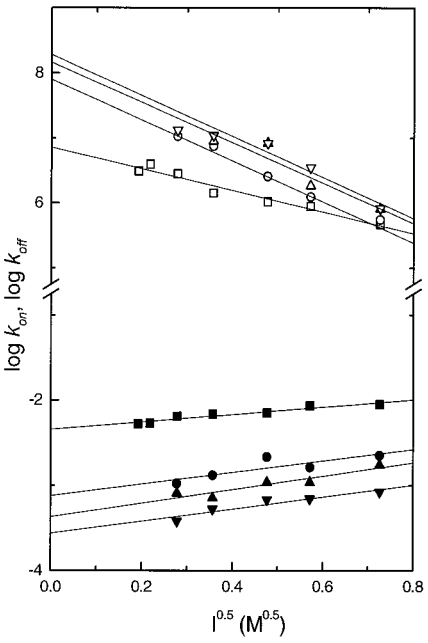

FIGURE 6: Debye−Hückel plot indicating the ionic strength dependence of the interaction between the various mutant MHF and actin. The plot shows the dependence of log k_{off} and log k_{on} on $\sqrt{I}$. The units for k_{on} and k_{off} are molar^{-1} second^{-1} and second^{-1}, respectively. All data were fitted to a straight line and extrapolated to zero ionic strength. The following slopes were measured for k_{off}: 0.43 for M765, 0.67 for M765(8/+4), 0.78 for M765(11/+6), and 0.70 for M765(20/+12). The intercepts were −2.35 in the case of M765, −3.12 for M765(11/+6), −3.37 for M765(11/+6), and −3.56 for M765(20/+12). Plots of log k_{on} against $\sqrt{I}$ gave lines with the following slopes: −1.27 $M^{-0.5}$ for M765, −3.13 $M^{-0.5}$ for M765(8/+4), −3.11 $M^{-0.5}$ for M765(11/+6), and −3.15 $M^{-0.5}$ for M765(20/+12). The intercepts were 6.63 for M765, 7.90 for M765(8/+4), 8.16 for M765(11/+6), and 8.28 for M765(20/+12). Since values for K_d are not independent from the rate constants, the plot of log K_d vs $\sqrt{I}$ is not shown. However, the plot gave slopes/intercepts of 2.08 $M^{-0.5}$/−9.19 for M765, 3.73 $M^{-0.5}$/−11.01 for M765(8/+4), 3.88 $M^{-0.5}$/−11.47 for M765(11/+6), and 3.66 $M^{-0.5}$/−11.73 for M765(20/+12). The rate constants for the actin−myosin interaction as well as the dissociation constant at zero ionic strength can be calculated from the intercepts and are shown in Table 4. Conditions: 20 mM Mops, 5 mM $MgCl_2$, and variable KCl concentrations, pH 7.0, 20 °C. Data for k_{off} are shown with solid filled symbols and for k_{on} with open symbols: M765 (■, □), (M765(8/+4) (●, ○), M765 (11/+6) (▲, △), and M765 (20/+12) (▼, ▽).

dissociation rate constant (k_{off}) by a factor of 5−15, suggesting that the charge on loop 2 plays a role in both the formation and stabilization of the actomyosin complex. It is noticeable that the differences between the three constructs with extra charge are small for both k_{on} and K_{app} but larger for k_{off}.

The ATPase studies show a greater than 10-fold change in K_{app} and relatively small changes in k_{cat}. Reliable estimates for steady-state parameters for M765 or *D. discoideum* myosin II are difficult to obtain as this requires very high actin concentrations. However, the values for M765(20/+12) are well-defined, and without change in k_{cat} the K_{app} for M765 would have to be close to 500 μM, much higher than any published estimate**.** The observed 2−3-fold increase in k_{cat} is small in energetic terms but implies that changes in loop 2 can affect the interaction of the myosin motor with nucleotide**.** There is no general agreement on the rate-limiting step of the actin-activated ATPase in solution, but it is normally thought to be associated with a conformational change associated with product release. However, it is clear that for fast muscle myosin at low ionic strength it is the rate of the ATP cleavage step (*37*).

Molecular genetic and biochemical modifications of loop 2 have been shown to alter myosin's affinity for actin and its actin-activated ATPase activity (*4*, *6*, *7*, *14*). Similarly, mutations at the negatively charged amino terminus of actin affect both myosin's affinity and its actin-activated ATPase activity (*16*, *17*). This is consistent with these two sites being complementary in the actomyosin interface and charge−charge interactions playing an important role in the binding of myosin to actin. Structural and functional studies have shown a remarkable conservation in the way in which actin and myosin isoforms from different species interact. The three-dimensional atomic models of F-actin decorated with *D. discoideum* S1 and F-actin decorated with rabbit chymotryptic S1 are very similar, suggesting a constancy of structure of the actomyosin complex and of the details of the molecular contacts at the actomyosin interface (*11*, *12*). In regard to function, every heterologous mixture of actin and myosin tested so far shows productive interaction. For instance, *D. discoideum* actin and rabbit skeletal muscle actin move at about 2 μm s^{-1} along *D. discoideum* myosin, and both forms of actin move at about 5 μm s^{-1} along rabbit skeletal muscle myosin (*38*). Therefore, it seems reasonable to assume that the molecular nature of the docking process with actin is similar for rabbit skeletal muscle myosin and *D. discoideum* myosin II. Thus binding to actin can be discussed in terms of the three-state docking model originally formulated for skeletal muscle myosin (*10*).

Scheme 2

$$\underset{}{A + M(\cdot N)} \overset{K_0}{\rightleftharpoons} \underset{\text{collision complex}}{A\sim M(\cdot N)} \overset{K_1}{\rightleftharpoons} \underset{\text{A state}}{A-M(\cdot N)} \overset{K_2}{\rightleftharpoons} \underset{\text{R state}}{A\cdot M(\cdot N)}$$

In this model the initial formation of a collision complex is governed by long-range ionic interactions and is strongly dependent on ionic strength but independent of temperature. The following isomerization to the A-state, leading to the formation of stereospecific hydrophobic interactions, is affected by organic solvent and temperature. Ionic strength has a comparatively small effect on the formation of the A-state. The final A-to-R transition involves major structural rearrangements with formation of additional A−M contacts and internal conformational changes involving both hydrophobic and ionic interactions. This transition results in

tighter actin binding and weaker nucleotide binding and is affected by ionic strength and solvent changes but little affected by temperature. In this model $k_{on} = K_0k_{+1}$ and $k_{off} = k_{-1}/(1 + K_2)$. The introduction of extra lysine residues in loop 2 is therefore expected to contribute to an increase in both K_0 and K_2, which is in good agreement with the observed results. Moreover, the effect of the extra charge in loop 2 is similar for K_0k_{+1} and K_{app}. This is consistent with K_{app} being controlled by the same charge−charge interaction that affects K_0, which was one of the original postulates of the model of Geeves, Goody, and Gutfreund (*39*).

Recent studies of the salt dependence of protein−protein interactions have suggested that such a mechanism may be quite general for the association between oppositely charged proteins (*40*). The association of proteins carrying complementary charges is thought to proceed through the formation of a low-affinity collision complex, which in terms of the analysis of Schreiber and Fersht (*40*) would be more correctly called a transition state. The initial low-affinity nonspecific complex is dominated and held together by long-range electrostatic interactions, before a second phase of more specific docking of the two interfaces leads to the formation of a high-affinity complex.

In an attempt to better understand the contribution of charge to the actin−myosin interaction, we studied the effect of ionic strength on k_{on} and k_{off}. For k_{on} the predicted values for all constants at zero ionic strength were much lower than those expected for a diffusion-controlled reaction, consistent with the value of k_{on} being a complex term comprised of more than one intrinsic rate constant (K_0k_{+1}). The slope of the Debye−Hückel plot was similar for all constructs with more than two extra lysine residues in loop 2 but significantly greater than for M765, suggesting that the increase in charge from 4 to 12 makes little contribution to k_{on} or to K_{app}. The slopes for k_{off} were all relatively small, suggesting little solvent shielding of the ionic interactions involved.

Detailed interpretation of such ionic strength dependencies in terms of electrostatic interactions is not simple. For the interaction between two molecules in solution, the slope of the Debye−Hückel plot is related to the strength of the ionic interaction and for point charges gives the number of interacting charges. Thus the ionic strength dependence of k_{on} and k_{off} gives an estimate of the extent to which such ionic interactions are shielded by solution ions and the extrapolation to zero ionic strength estimates the constants in the absence of any solution shielding. As the protein molecules used here are identical except for the changes in loop 2, a change in the number of charges involved in the protein−protein interface might be expected to result in a change in the slope of the Debye−Hückel plot. The remarkable result from the data in Figure 6 for k_{on} is that there are relatively small changes in slope between the three constructs with 4−12 extra charges. However, the binding reaction is known to occur in multiple steps and we are measuring complex terms K_0k_{+1} and $k_{-1}/(1 + K_2)$, not a simple diffusion-limited association reaction. Thus the exact effects of the charge change are difficult to predict.

The specific goal of this study was to understand how changes in the structure and charge of loop 2 affect the enzymatic behavior of a mutant myosin and its interaction with actin. Our analysis of the nine mutant constructs reveals a clear correlation between the charge of the loop, the activation by actin of the mutant constructs' ATPase rates, and the strength of the interaction between mutant motor domains and actin. The charge changes used in our study are large in comparison with those in previous studies using chimeric substitutions of loop 2 sequences (*6*, *7*). However, the loop 2 sequences from skeletal and cardiac muscle used in these studies have an asymmetric distribution of basic and acidic amino acid residues. This leads to the clustering of five lysine residues at the C-terminal end of the loop, at an ideal position for interaction with actin, without increasing the net charge of the molecule by more than one positive charge. One final point of interest in these constructs is the usefulness of a myosin head with an actin affinity of 40 pM and a $K_{app} < 10\ \mu$M for further studies. One of the major problems of structural studies of the actomyosin complex is that while the rigor complex has been well-characterized, the actomyosin complex in the presence of ATP, which is thought to represent the pre-power-stroke state, has been difficult to study in solution because of its short lifetime and very low actin affinity. The myosin constructs created here maybe of great interest for structural studies of the ternary actomyosin·ATP complex.

ACKNOWLEDGMENT

We thank S. Zimmermann for expert technical assistance and the generation of expression vectors for the mutant constructs; M. Knetsch for the gift of M765; G. Helmig and N. Adamek for preparation of actin and pyr-actin; J. Biosca, M. Knetsch, H. Pöpperl, J. Wray, and S. Kurzawa for critical reading of the manuscript and discussions; and R. S. Goody and K. C. Holmes for continual support and encouragement.

REFERENCES

1. Rayment, I., Rypniewski, W. R., Schmidt-Bäse, K., Smith, R., Tomchick, D. R., Benning, M. M., Winkelmann, D. A., Wesenberg, G., and Holden, H. M. (1993) *Science 261*, 50−58.
2. Fisher, A. J., Smith, C. A., Thoden, J. B., Smith, R., Sutoh, K., Holden, H. M., and Rayment, I. (1995) *Biochemistry 34*, 8960−8972.
3. Spudich, J. A. (1994) *Nature 372*, 515−518.
4. Yamamoto, K. (1991) *J. Mol. Biol. 217*, 229−233.
5. Kelley, C. A., Takahashi, M., Yu, J. H., and Adelstein, R. S. (1993) *J. Biol. Chem. 268*, 12848−12854.
6. Uyeda, T. Q. P., Ruppel, K. M., and Spudich, J. A. (1994) *Nature 368*, 567−569.
7. Rovner, A. S., Freyzon, Y., and Trybus, K. M. (1995) *J. Biol. Chem.* 270**,** 30260−30263.
8. Perreault-Micale, C. L., Kalabokis, V. N., Nyitray, L., and Szent-Gyorgyi, A. G. (1996) *J. Muscle Res. Cell Motil. 17*, 543−553.
9. Bobkov, A. A., Bobkova, E. A., Lin, S. H., and Reisler, E. (1996) *Proc. Natl. Acad. Sci. U.S.A. 93*, 2285−2289.
10. Geeves, M. A., and Conibear, P. B. (1995) *Biophys. J. 68*, 194S−199S.
11. Rayment, I., Holden, H. M., Whittaker, M., Yohn, C. B., Lorenz, M., Holmes, K. C., and Milligan, R. A. (1993) *Science 261*, 58−65.
12. Schröder, R. R., Manstein, D. J., Jahn, W., Holden, H., Rayment, I., Holmes, K. C., and Spudich, J. A. (1993) *Nature 364*, 171−174.
13. Bonafe, N., Chaussepied, P., Capony J. P., Derancourt J., and Kassab, R. (1993) *Eur. J. Biochem. 213*, 1243−1254.
14. Chaussepied, P., and Morales, M. F (1988) *Proc. Natl. Acad. Sci. U.S.A. 85*, 7471−7475.

15. Aspenstrom, P., and Karlsson, R. (1991) *Eur. J. Biochem. 200*, 35−41.
16. Sutoh, K., Ando, M., and Toyoshima, Y. Y. (1991) *Proc. Natl. Acad. Sci. U.S.A. 88*, 7711−7714.
17. Cook, R. K., Root, D., Miller, C., Reisler, E., and Rubenstein, P. A. (1993) *J. Biol. Chem. 268*, 2410−2415.
18. Ritchie, M. D., Geeves, M. A., Woodward, S. K. A., and Manstein, D. J. (1993) *Proc. Natl. Acad. Sci. U.S.A. 90*, 8619−8623.
19. Kurzawa, S. E., Manstein, D. J., and Geeves, M. A. (1997) *Biochemistry 36*, 317−323.
20. Marston, S. B., and Taylor, E. W. (1980) *J. Mol. Biol. 139*, 573−600.
21. Sambrook, J., Fritsch, E. F., and Maniatis, T. (1989) *Molecular cloning: a laboratory manual*, Cold Spring Harbor Laboratory Press, Cold Spring Harbor, NY.
22. Manstein, D. J., Schuster, H.-P., Morandini, P., and Hunt, D. M. (1995) G*ene 162*, 129−134.
23. Perrin, S., and Gilliland, G. (1990) *Nucleic Acids Res. 18*, 7433−7438.
24. Egelhoff, T. T., Titus, M. A., Manstein, D. J., Ruppel, K. M., and Spudich, J. A. (1991) *Methods Enzymol. 196*, 319−334.
25. Manstein, D. J., and Hunt, D. M. (1995) *J. Muscle Res. Cell Motil. 16*, 325−332.
26. Lehrer, S. S., and Kewar, G. (1972) *Biochemistry 11*, 1211−1217.
27. Criddle, A. H., Geeves, M. A., and Jeffries, T. (1985) *Biochem. J. 232*, 343−349.
28. Trentham, D. R., Bardsley, R. G., Eccleston, J. F., and Weeds, A. G. (1972) *Biochem. J. 126*, 635−644.
29. White, H. D. (1982) *Methods Enzymol. 85*, 698−708.
30. Giese, K. C., and Spudich, J. A. (1997) *Biochemistry 36*, 8465−8473.
31. Marston, S. B. (1982) *Biochem. J. 203*, 453−460.
32. Kurzawa, S. E., and Geeves, M. A. (1996) *J. Muscle Res. Cell Motil. 17*, 669−676.
33. Marston, S., and Weber, A. (1975) *Biochemistry 14*, 3868−3873.
34. Coates, J. H., Criddle, A. H., and Geeves, M. A. (1985) *Biochem. J. 232*, 351−356.
35. Konrad, M., and Goody, R. S. (1982) *Eur. J. Biochem. 128*, 547−555.
36. Siemankowski, R. F., and White, H. D. (1984) *J. Biol. Chem. 259*, 5045−5053.
37. White, H. D., Belknap, B., and Webb, M. R. (1997) *Biochemistry 36*, 11828−11836.
38. Kron, S. J., and Spudich, J. A. (1986) *Proc. Natl. Acad. Sci. U.S.A. 83*, 6272−6276.
39. Geeves, M. A., Goody, R. S., and Gutfreund, H. (1984) *J. Muscle Res. Cell Motil. 5*, 351−361.
40. Schreiber, G., and Fersht, A. R. (1996) *Nat. Struct. Biol. 3*, 427−431.
41. Levitt, M. (1992) *J. Mol. Biol. 226*, 507−533.
42. Sayle, R. A., and Milner-White, E. J. (1995) *Trends Biochem. Sci. 20*, 374.

BI972851Y